Medina, J.; Perez, P.; Garces, G.; Stark, A.; Schell, N.; Adeva, P.:
High-strength Mg-6Zn-1Y-1Ca (wt%) alloy containing quasicrystalline I-phase processed by a powder metallurgy route
In: Materials Science and Engineering A 715 (2018) 92 - 100
First published online by Elsevier: January 1, 2018

DOI: 10.1016/j.msea.2017.12.111
https://dx.doi.org/10.1016/j.msea.2017.12.111

High-strength Mg-6Zn-1Y-1Ca (wt%) alloy containing quasicrystalline I-phase processed by a powder metallurgy route

J. Medina[a], P. Pérez[a,*], G. Garcés[a], A. Stark[b], N. Schell[c], P. Adeva[a]

[a] Department of Physical Metallurgy, National Center for Metallurgical Research (CENIM-CSIC), Avda. Gregorio del Amo 8, 28040 Madrid, Spain

[b] Institute of Materials Research, Helmholtz-Zentrum Geesthacht, Max-Planck-Str. 1, 21502 Geesthacht, Germany

[c] Structural Research on New Materials, Helmholtz-Zentrum Geesthacht Outstation at DESY, Hamburg, Germany

[*] Corresponding author:
E-mail address: zubiaur@cenim.csic.es (P. Pérez)

Keywords
Mg-Zn-Y alloys Powder metallurgy Microstructure Mechanical properties

Abstract

A high-strength Mg-6Zn-1Y-1Ca (wt%) alloy has been processed by a powder metallurgy route. Rapidly solidified powders with a particle size below 100 μm were used as a way for preventing formation of ternary MgZnCa compounds during subsequent extrusion at 250 °C. The microstructure of the extruded alloy consists of an ultrafine-grain magnesium matrix, with an average grain size of 444 nm, embedding a high volume fraction of fine I-phase particles aligned along the extrusion direction. The alloy combines an excellent ductility (14% of elongation to failure) with a high strength (ultimate strength of 469 MPa and yield stress of 461 MPa) at room temperature, mainly due to grain size refinement (around 70% of the yield stress). The strength is kept high up to 150 °C (yield stress of 279 MPa). Above this temperature, the mechanical strength falls to very low values but the ability to deform plastically is considerably enhanced, exhibiting superplastic behaviour from 200 to 350 °C, with a maximum elongation of 477% at 350 °C.

1. Introduction

Magnesium alloys are the most attractive candidates for structural applications where weight saving constitutes an important design parameter because they are one of the lightest structural metallic materials. However, their use in most of applications is still limited because of their low ductility at room temperature, insufficient strength at intermediate and high temperatures and poor corrosion resistance. In order to overcome these problems efforts are being dedicated to modify the microstructure of alloys through the proper choice of alloying elements [1–5] and/or optimizing their processing [6–11]. A great number of potential high-strength alloy families have been developed by adjusting the composition of magnesium alloys. In this way, alloys based on ternary Mg-Zn-Y family offer many possibilities for producing high strength alloys because the alloy can be reinforced by different intermetallic phases, being the maximum hardening induced by the quasicrystalline I-phase [12–17] or a long period stacked ordered phase (designated as LPSO-phase) [18–21]. The alloys containing these thermally stable second phases combine excellent ductility at room temperature with high strength up to 200–250 °C [12–22]. Major advantage of the use of alloys reinforced by the I-phase compared to that strengthened by the LPSO-phase is the firsts are cheaper because of the lower content in alloying elements, especially in yttrium. The quasiperiodic crystal structure of the I-phase offers the advantage of a strong interface with the magnesium matrix, conferring high hardness and strength to magnesium alloys. Furthermore, its low interfacial energy prevents its coarsening

during exposure at elevated temperatures, so I-phase is very effective refining the grain size of magnesium alloys.

The addition of a new element to the Mg-Zn-Y alloys can result in an additional improvement of their mechanical strength. Particularly, the beneficial effect of calcium additions on the mechanical properties at room temperature and creep resistance has been reported [23–25], with the advantage that calcium additions tend to reduce the strong basal texture typical of wrought magnesium alloys by favouring homogeneous recrystallization during extrusion process [22]. Moreover, calcium also increases the ignition temperature of magnesium alloys [26,27]. Once considered the benefits of Ca alloying, the next step regards the choice of the more appropriated thermo-mechanical processing route. This point is critical to achieve a fine microstructure in which the second phases are homogeneously dispersed inside the magnesium matrix. The use of a powder metallurgy (PM) route involving consolidation by extrusion of rapidly solidified (RS) powders appears as the right approach to attain the objective of refining the microstructure of these alloys [11,15,28–32]; ultimate tensile strengths (UTS) around 450 MPa for alloys containing the I-phase [33] and close to 600 MPa for alloys reinforced by the LPSO-phase [34]. Therefore, the present research is focused on increasing the strength of the Mg-6Zn-1Y-1Ca (wt%) alloy between room temperature and 200 °C through a powder metallurgy route involving the extrusion of rapidly solidified powders. A complete study on the extruded bars about the influence of Ca additions on the microstructure, the evaluation of the mechanical properties between room temperature and 350 °C and the analysis of the different reinforcing mechanisms contributing to the high strength of the extruded PM alloy have been done.

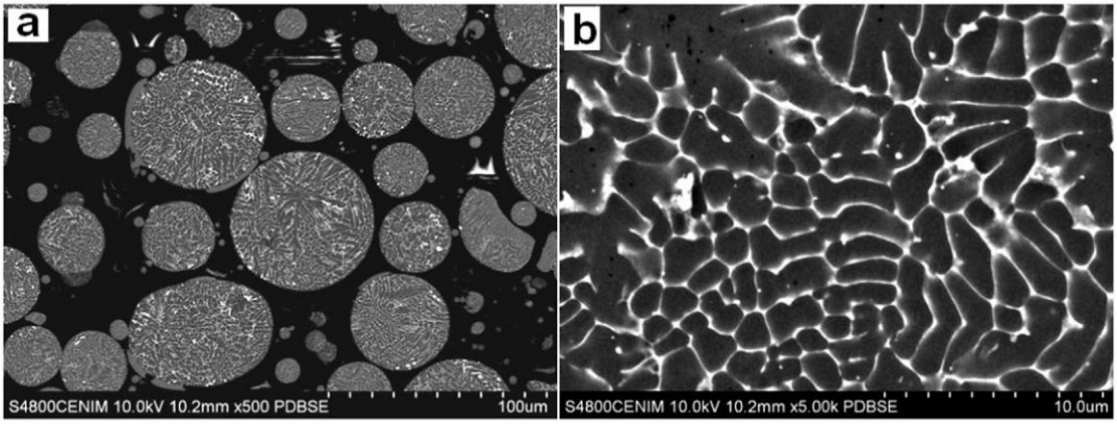

Fig. 1. Backscattered electron images of rapidly powder particles of Mg-6Zn-1Y-1Ca alloy. (a) General view, (b) detail of the dendritic structure.

2. Experimental

The alloy, with a nominal composition of Mg-6Zn-1Y-1Ca (wt%) (corresponding to Mg-2.3Zn-0.3Y-0.6Ca in atomic percentage), was prepared by melting pure elements in a resistance furnace and poured into cylindrical molds 42 mm in diameter. Spherical rapidly solidified (RS) powders less than 200 μm in diameter were fabricated from as-cast bars by TLS Technik GmbH (Germany) using electrode inductionmelting gas atomization (EIGA) technique. The powders were isostatically cold pressed in 40 mm diameter compacts and then extruded at 250 °C using an extrusion ratio of 18:1.

Microstructural observations were carried out by scanning electron microscopy (SEM) and transmission electron microscopy (TEM), using a Hitachi S-4800 and a Jeol-2010, respectively. Both microscopes were equipped with an energy-dispersive X-ray microanalysis (EDS). The thermal stability of the extruded bars was monitored through differential scanning calorimetric (DSC) experiments in which high energy synchrotron radiation diffraction (HEDRX) patterns where simultaneously recorded in the course of DSC tests. These measurements were carried out at the P07 beam-line of PETRA III, at the Deutsches Elektronen-Synchrotron (DESY). The sample was encapsulated in stainless steel crucible employing an empty crucible as reference. The DSC unit was positioned inside the coil of a DIL805A/D dilatometer which was modified for synchrotron experiments, having a hole that allows the incidence of X-ray beam in the sample. The measurements were performed under an argon flow. The beam energy was 87.1 KeV, corresponding to a wavelength of 0.01424 nm. The diffraction patterns were recorded using a 2D Perkin Elmer XRD 1621 flat panel detector placed 2350 mm from the sample, with an array of 20482 pixels and 200 μm2 pixel size.

LaB6 standard powder sample was employed to calibrate the acquired diffraction spectra. The sample was exposed to one DSC cycle from room temperature up to 700 °C with a heating rate of 20 °C/min and then cooled down to room temperature. Conventional diffraction patterns as a function of 2θ were obtained by integration of Debye-Scherrer rings using Fit2D software.

X-ray diffraction (XRD) using Co-Kα radiation was used for texture measurements. Measurements were carried out in Siemens D5000 X-ray diffractometer (XRD) and texture data were analyzed by TextEval software. Metallographical preparation for SEM observation included mounting of the extruded sample in Bakelite, conventional mechanical polishing with different alumina suspensions and final polishing with colloidal silica solution. Specimens for TEM observations were prepared by electrolytic jet polishing using as reactive a mixture of 25% nitric acid and 75% methanol at −20 °C and 20 V. A final ion milling step at liquid nitrogen temperature was used to remove any thin oxide film formed on samples during electrolytic polishing. Measurements of grain size, volume fraction of second phases, particles and precipitates sizes were determined by TEM micrographs using Sigma Scan Pro software.

Mechanical properties of the extruded Mg-Zn-Y-Ca alloy were evaluated by tensile tests. Cylindrical samples (radius 3 mm and gauge length of 10 mm) were machined from the extruded bar, with their longer dimension parallel to the extrusion direction. Tensile tests were performed in a universal tensile machine under a constant cross-head speed condition at an initial strain rate of 10^{-4} s^{-1} from room temperature up to 350 °C. Additional tests at temperatures higher than 200 °C were carried out at higher strain rates. The stress exponent was determined through jump strain rate tests. In these tests, the sample is initially deformed at a given strain rate until a steady state is attained. At this point the strain rate is increased/reduced until a new steady state is reached. Successive changes in the strain rate following this procedure were carried out at strain rates comprised between 10^{-5} and 10^{-1} s^{-1}.

3. Results

3.1. Microstructural characterization

The metallographic section of RS powders is presented in Fig. 1, showing a dendritic microstructure independently of the particle size although the dendrite size decreases as the size of the particle becomes smaller. The high cooling rates achieved during solidification results in a supersaturated metastable dendritic structure in which magnesium dendrites and interdendritic regions consist of a solid solution of the different alloying elements in the magnesium lattice. Semiquantitative EDS microanalyses (listed in Table 1) reveal high contents of all alloying elements in the interdendritic regions, in concentrations three times higher than those measured in the dendrites.

The metastable microstructure of atomized powders evolves during the extrusion stage, as observed in Fig. 2. Interdendritic regions breakdown results in the precipitation of second-phase particles which are aligned along the extrusion direction (ED) (Fig. 2a). The volume fraction of second phases located at grain boundaries is 15% while is 0.2% for finer precipitates within the magnesium grains. The matrix (dark phase) corresponds to practically pure magnesium dissolving small amounts of zinc whereas calcium and yttrium are practically absent (see Table 2). On the other hand, bright magnesium-rich secondphase particles contain relevant amounts of zinc, yttrium and calcium which coincide rather well with those measured at interdendritic regions in RS powders. The material can be considered fully dense because only a small volume fraction of porosity, 0.03±0.01%, is found.

Table 1
Chemical composition (at%) of the phases found in Mg-6Zn-1Y-1Ca RS powders.

	Mg (at%)	Zn (at%)	Y (at%)	Ca (at%)
Dendrite	96.8	2.5	0.2	0.5
Interdendritic region	91.3	6.2	0.7	1.8

Table 2
Chemical composition (at%) of the phases found in the extruded Mg-6Zn-1Y-1Ca alloy.

	Mg (at%)	Zn (at%)	Y (at%)	Ca (at%)
Matrix	97.1	2.3	0.2	0.4
Second phase	90.2	7.4	1.0	1.4

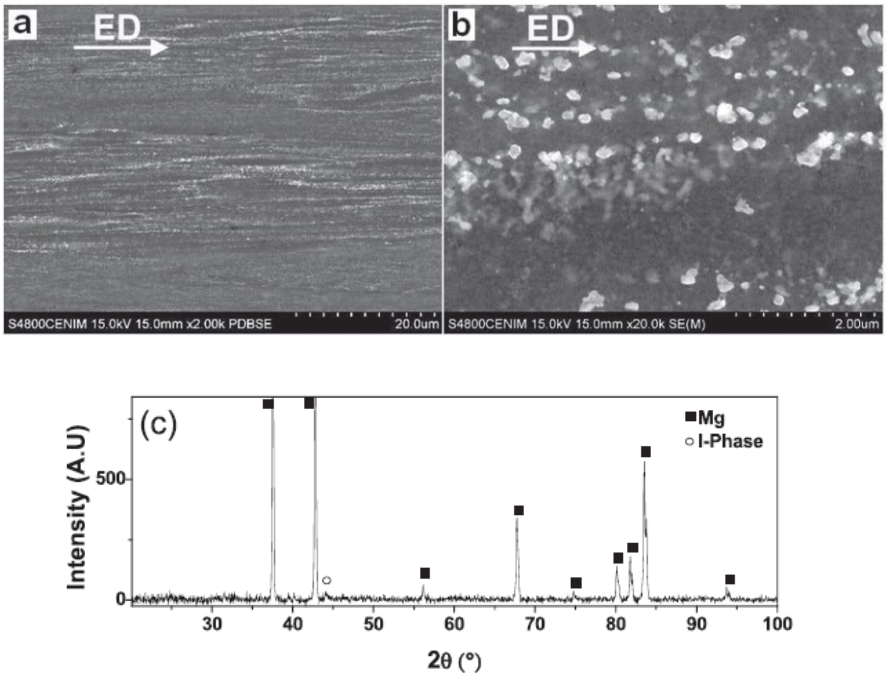

Fig. 2. Backscattered electron images showing the microstructure of extruded Mg-6Zn-1Y-1Ca bars. (a) General view, (b) detail of second phases aligned along the extrusion direction. (c) XRD pattern showing the phases existing in the alloy.

Fig. 3 shows the DSC curve of the extruded Mg-6Zn-1Y-1Ca alloy at a heating rate of 20 °C/min. Three endothermic peaks can be found at 389, 508 and 617 °C. In situ HEDRX patterns presented in Fig. 4 allow identifying the second phases of the extruded alloy and their evolution during heating in the DSC experiment. At room temperature and up to 300 °C the main phases existing in the alloy are Mg and I-phase. The I-phase dissolves significant amount of calcium, as deduced from EDS microanalyses. Major changes in the nature of second phases occur above 300 °C. Beyond this temperature, peaks due to intermetallic Mg6Zn3Ca2 compound and W-phase appear simultaneously instead of I-phase peaks. As can be seen in HEXRD patterns of Fig. 4, Mg6Zn3Ca2 disappears at 390 °C. This temperature coincides with the melting of this phase in the first endothermic peak of the DSC curve and it is in agreement with the melting temperature reported for the Mg6Zn3Ca2 phase in Mg-Zn-Ca alloys [35–37]. On the other hand, W-phase remains stable up to about 470 °C (Fig. 4). The transformation associated with the melting of this phase corresponds to the second endothermic peak in the DSC curve (Fig. 3) and it matches with W-phase melting [37–39]. As intensity of W-phase decreases, new small peaks of a non-identified phase appears in the temperature range 400–510 °C (see Fig. 4). This suggests that dissolution of ternary Mg6Zn3Ca2 phase promotes gradual dissolution of the W-phase in a new phase stable up to about 510 °C, in agreement with the small peak found in the DSC curve at 508 °C. The most intense peak at 617 °C in DSC curve corresponds to the melting of the magnesium matrix.

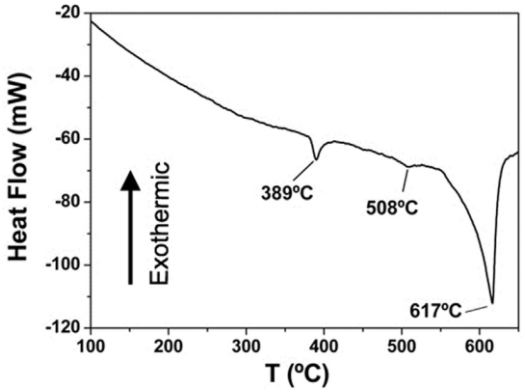

Fig. 3. DSC curve during heating at 20 °C/min of extruded Mg-6Zn-1Y-1Ca alloy.

Bright field TEM micrographs of Fig. 5 show a more detailed view of the microstructure. The average grain size of the magnesium matrix calculated from TEM images is 444 nm, as shown in the histogram of Fig. 6. Second phases are located within the magnesium grains as well as at grain boundaries. Coarse irregular second phases, with an average size of 83 nm, are mainly placed at grain boundaries (see Fig. 5a) while finer spherical particles with an average size of 15 nm are mostly distributed inside the magnesium grains (see Fig. 5b). The volume fraction of spherical particles is 0.2%. According to EDS microanalyses in TEM, coarse irregular particles contain zinc, yttrium and calcium. Their stoichiometry is close to that of the I-phase, in good agreement with the phase detected in HEXRD patterns. On the contrary, the small spherical particles are enriched in zinc, but also contains minor amounts of yttrium and calcium.

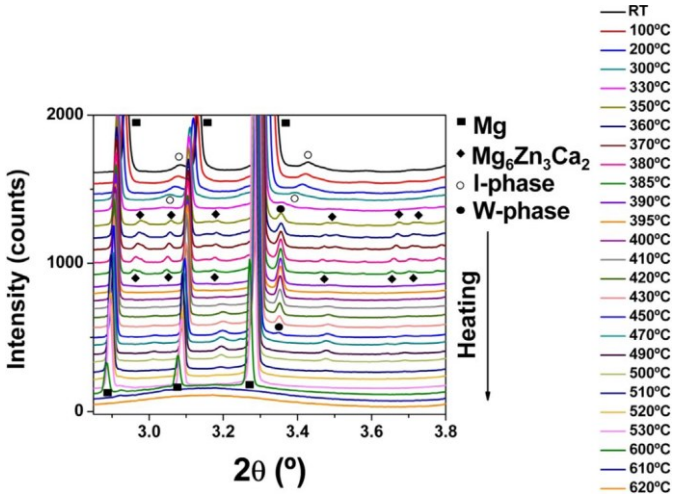

Fig. 4. Synchrotron diffraction patterns for extruded Mg-6Zn-1Y-1Ca alloy taken “in-situ” during heating at 20 °C/min.

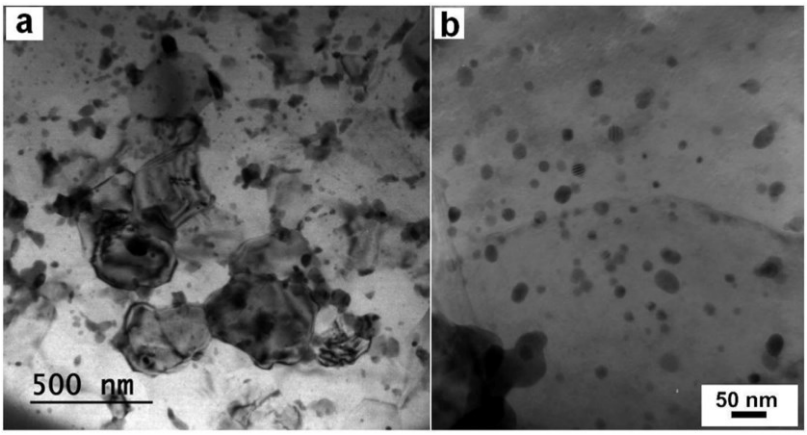

Fig. 5. TEM bright field images of Mg-6Zn-1Y-1Ca alloy showing; (a) coarse irregular second phases at magnesium grain boundaries and (b) fine round particles inside the magnesium grains.

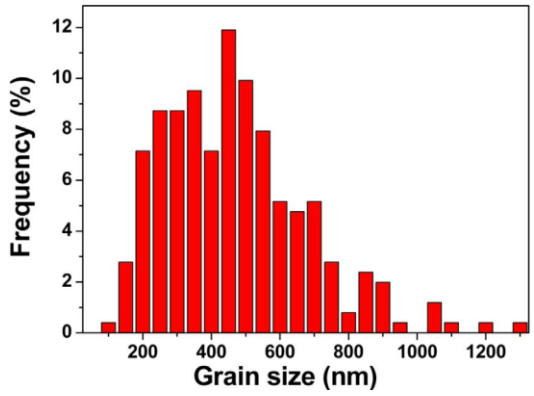

Fig. 6. Grain size histogram of Mg-6Zn-1Y-1Ca alloy.

Texture analysis was carried out by XRD measurements. The calculated pole figures for basal {0001} and prismatic {1010} planes are presented in Fig. 7. Pole figures reveal certain basal texture in which basal planes are parallel to the extrusion direction (ED), along the diameter of the extruded bar (TD), with a maximum intensity of 4 and 5 for the {0001} and {1010} pole figures, respectively. The relatively weak texture existing in the bars results not only from calcium additions, as found in the literature [40], but also by the fine equiaxed structure of the magnesium grains in the extruded material.

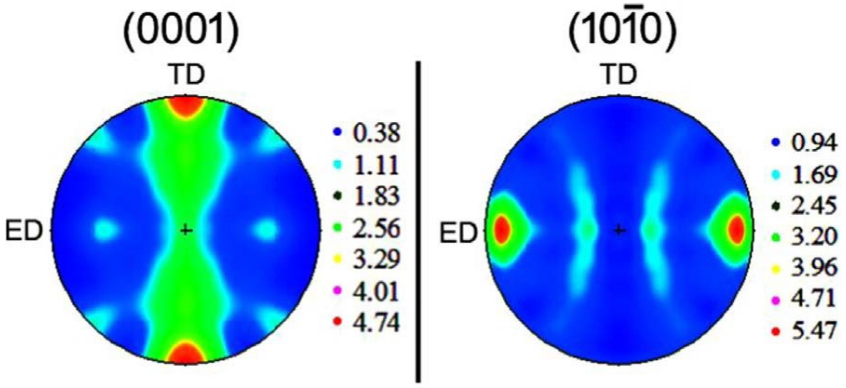

Fig. 7. Calculated pole figures in the basal plane {0001} and prismatic plane {1010} of the extruded PM Mg-6Zn-1Y-1Ca alloy.

3.2. Mechanical characterization

Mechanical behaviour was evaluated by tensile tests. True stress–true strain and engineering stress-engineering strain curves from room temperature to 350 °C are plotted in Fig. 8 while numerical values of yield stress, UTS and elongation to failure are listed in Table 3. Depending on test temperature different behaviours can be identified in tensile curves. The alloy exhibits very high strength up to 150 °C (Fig. 8a). Tensile curves display a yield point phenomenon within this temperature range, probably associated with the pinning effect for dislocation motion of fine second-phase particles. The maximum strength coincides with the upper yield stress and then the stress drops about 15 MPa to the lower yield stress. As yield stress was considered the mean value of the upper and lower yield stress, i.e. 461 MPa. Beyond the lower yield stress, during plastic deformation, there is some hardening at room temperature and softening at 100 and 150 °C. At room temperature, the UTS is 469 MPa with an elongation to failure of 14%. The strength of the alloy decreases with increasing the temperature but it is kept close to 300 MPa at 150 °C but ductility is considerably enhanced (elongation to failure of 43% at 150 °C).

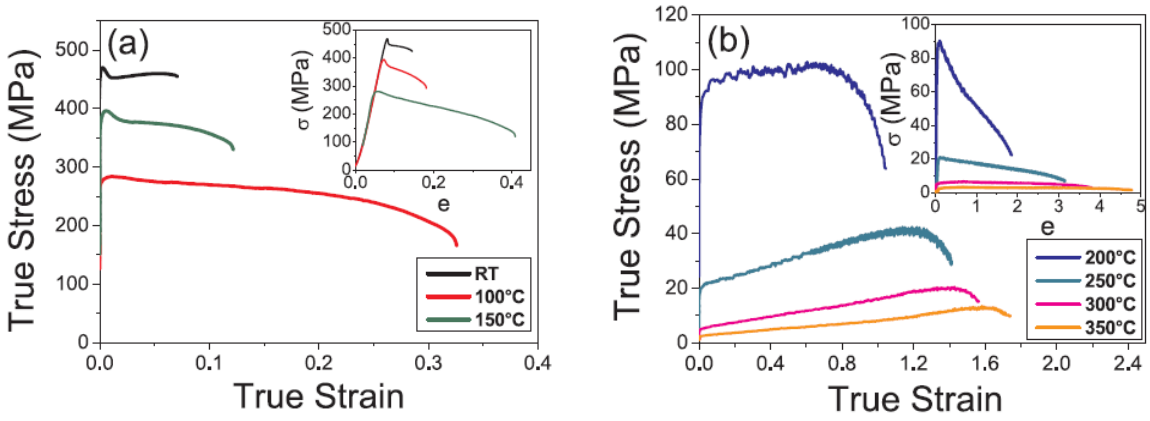

Fig. 8. True stress-true strain curves of Mg-6Zn-1Y-1Ca alloy. (a) RT-150 °C temperature range and (b) 200–350 °C temperature range. The insets plot the engineering stress-strain curves.

Table 3
Yield stress (YS), ultimate tensile strength (UTS) and elongation to failure (EF) values of the extruded Mg-6Zn-1Y-1Ca alloy tensile tested from room temperature up to 350 °C.

Temperature (°C)	YS (MPa)	UTS (MPa)	EF (%)
25	461	469	14
100	386	396	18
150	279	285	43
200	70	102	200
250	17	42	344
300	5	20	379
350	2	13	477

Above 150 °C the stress falls to very low values; 70 MPa at 200 °C and below 30 MPa above this temperature. Nevertheless, the ductility of the alloy exceeds values higher than 200%, with a maximum elongation of 477% at 350 °C (Fig. 8b). Tensile curves in this temperature range present a long steady state, showing a pronounced hardening as the test temperature is increased, probably, due to gradual grain coarsening during plastic deformation.

In order to determine deformation mechanisms operating at high temperatures, jump strain rate tensile tests in the 200–350 °C temperature range were carried out. Fig. 9 displays the strain rate-true stress dependence, plotted in a double logarithmic scale, according with the general power-law constitutive creep equation:

$\dot{\varepsilon} = k\sigma^{napp}e^{(-Qapp/RT)}$

where k is the creep constant, σ is the flow stress, napp is the apparent stress exponent, Qapp is the apparent activation energy, R is the universal gas constant and T is the absolute temperature.

Two strain rate regimens can be clearly distinguished at all temperatures: In the first regime napp is close to 5 while it takes values close 2–3 in the second regime. The regime with the low napp appears at low strain rates at low temperatures, tending to shift to higher strain rates as the temperature increases. Thus, napp at 200 °C is 2.9 at low strain rates (from 10−5 to 3.10–4 s−1) and 11 at higher strain rates (from 10−3 to 10−1 s−1). At 250 °C at strain rates between 3.10–4 and 3.10−3 s−1, however, low napp regime appears (napp ≈ 2.6), sandwiched between two regions with napp ≈ 5. Above this temperature, the transition from the high napp regime (napp ≈ 5) to the low napp regime (napp ≈ 2) takes place at 10−4 s−1 in such a way that low napp regime extends over the entire interval of high strain rates (from 10−4 to 10−1 s−1).

The activation energy has been calculated by the following equation:

$$Q_{app} = -R\left(\frac{\partial ln\dot{\varepsilon}}{\partial 1/T}\right)_{\sigma}$$

Qapp is 141 kJ/mol in the temperature range 200–350 °C in the low napp regime. This value is very close to the activation energy of lattice diffusion in magnesium (135 kJ/mol) [41].

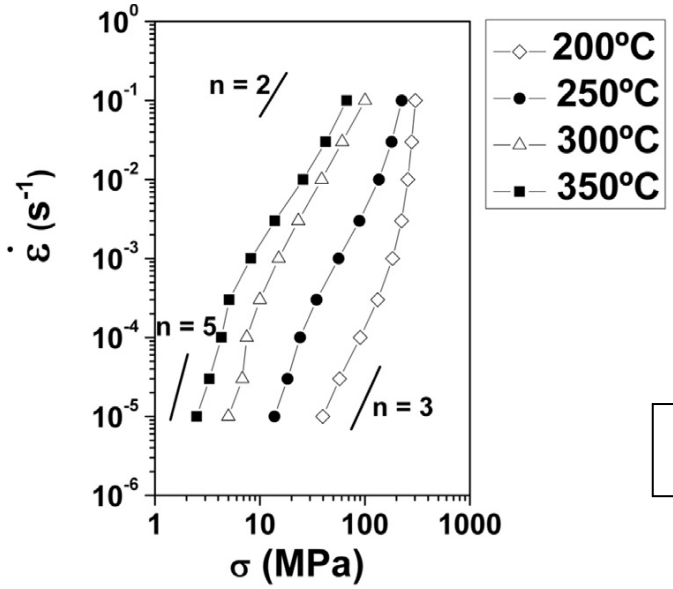

Fig. 9. Strain rate–true stress plot for the Mg-6Zn-1Y-1Ca alloy in the temperature range 200–350 °C.

4. Discussion

The use of rapidly solidified atomized powders promotes a marked grain refinement in the Mg matrix of the extruded bars. The high cooling rate achieved during atomization results in the development of a metastable dendritic microstructure in the rapidly solidified powders in which both the magnesium dendrites and interdendritic regions keep in solid solution high concentrations of all alloying elements, especially in the case of the interdendritic spaces. Such metastable microstructure has been also described in atomized powders of other magnesium alloys [6,30]. This metastable microstructure evolves during the extrusion process. The temperature used for extrusion, 250 °C, is high enough for breaking solid solution stability, resulting in a homogeneous precipitation throughout the alloy. Thus, the microstructure of the extruded bars consists of a fine-grained magnesium matrix, with an average grain size below 500 nm, reinforced by a fine dispersion of second phases. Two different morphologies can be distinguished: (i) Fine irregular blocky particles, mainly located at magnesium grain boundaries and (ii) nanosized spherical precipitates, mostly placed inside the magnesium grains, although they can be viewed at grain boundaries sporadically. This homogeneous distribution of second phases accounts for the considerable refinement of the microstructure achieved in the extruded bars because second-phase particles act during the extrusion process as effective pinning points for grain boundary migration of magnesium recrystallized grains.
According with EDS microanalysis and in-situ synchrotron diffraction patterns, atomization induces the formation of a metastable microstructure with a chemical composition close to that of the I-phase, but dissolving also small amounts of calcium. This microstructure, however, contrasts with that found for the same alloy processed by extrusion of as-cast rods [37]. In this case, coarse Mg6Zn3Ca2 and fine W-phase particles are located at grain boundaries of the magnesium matrix, appearing aligned along the extrusion direction. Small amounts of the I-phase are exclusively present within the magnesium grains as very fine precipitates. The formation of such phases was attributed to the effect of calcium modifying the stability range of W- and I- phases. Since W-phase and intermetallic Mg6Zn3Ca2 compound are not found in the microstructure of atomized powders, their absence has to be associated with a change in the nature of the phases existing in the alloy as result of the high cooling rates achieved during powder atomization. A fine metastable dendritic structure is developed, as noticed from the high amounts of alloying elements dissolved in the dendrites and especially, in the interdendritic regions. During the holding time at the extrusion temperature (15–20 min), the supersaturated solid solution in dendrites and interdendritic spaces is broken, just leading a fine precipitation of the I-phase which can dissolve small amounts of calcium. This microstructure is stable up to about 350 °C, temperature at which the I-phase transforms into stable Mg6Zn3Ca2 and W-phase. Probably, I-phase particles with higher calcium contents evolve towards Mg6Zn3Ca2 compound while those with higher yttrium contents evolve towards W-phase (Mg3Zn3Y2), as deduced from DSC and HEDRX patterns (Figs. 3 and 4). Furthermore, when heating is continued over the melting point of the alloy and then it is slow down cooling at 20 °C/min, far from rapid solidification conditions W-phase and Mg6Zn3Ca2 are formed instead I-phase, (see Fig. 10), in agreement with the behavior found for as-cast alloys [37].

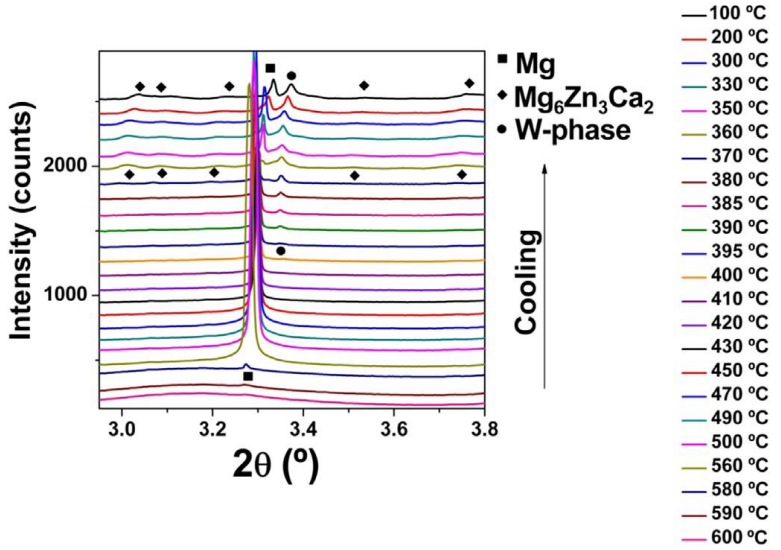

Fig. 10. Synchrotron diffraction patterns for extruded Mg-6Zn-1Y-1Ca alloy during cooling at 20 °C/min.

The fine-grained microstructure of the alloy accounts for the high yield stress and tensile strength of the alloy. Fine homogeneous precipitation of I-phase particles during the extrusion guarantees fine magnesium grains because they limit effectively grain growth. It is expected that grain refinement would constitute the main strengthening mechanism in this PM-alloy. Thus, the contributions due to the different hardening mechanism have been evaluated to validate such assumption.

The yield stress of the alloy (σ0.2) could be expressed as:

$$\sigma_{0.2} = V_m \cdot \sigma_m + V_{par} \cdot \sigma_{par} \quad (1)$$

Where σm is the yield strength of the magnesium matrix, σpar the yield stress of coarse second-phase particles and Vm and Vpar are the corresponding volume fractions of Mg and coarse second phases, respectively. In turn, the yield stress of the matrix σm results from three strengthening mechanisms: grain size refinement calculated by Hall- Petch equation, precipitate hardening according to Orowan equation and solid solution hardening.

$$\sigma_m = \sigma_{HP} + \sigma_{OR} + \sigma_{ss} \quad (2)$$

Table 4 lists microstructural parameters of the alloy used for determining the contribution due to the different strengthening mechanisms.

Table 4
Main microstructural parameters for the extruded Mg-6Zn-1Y-1Ca alloy: grain size (D), volume fraction of coarse second phases (Vpar), size of coarse second phases (dpar), volume fraction of precipitates (Vpp), size of precipitates (d).

D (nm)	Vpar (%)	dpar (nm)	Vpp (%)	dpp (nm)
444±2	15±2	83±16	0.22±0.03	15±1

4.1. Strengthening due to grain size

The grain size effect on the mechanical properties can be calculated through the Hall-Petch equation as follows:

$$\sigma_{HP} = \sigma_0 + K/D^{-1/2} \quad (3)$$

being σHP the influence of the grain size on the yield stress, σ0 is the friction stress, K is the grain boundary strengthening coefficient and D is the average grain size. Since the magnesium matrix is practically free of alloying elements, σ0 and K for a randomly oriented as-cast magnesium alloy were taken [42], whose values are 17.7 MPa and 0.25 MPa m−1/2, respectively. Calculated value for σHP in the Mg-6Zn-1Y-1Ca alloy, given a volume fraction of the magnesium matrix of 85%, is 333 MPa. The ultra-fine grain size (444 nm.) results in a high yield stress value due to the Hall-Petch effect.

4.2. Strengthening due to fine precipitates

The Mg-6Zn-1Y-1Ca alloy contains a significant amount of small particles (volume fraction of 0.2%) with spherical morphology within the magnesium grains (Fig. 5b). These particles could act as effective barriers for dislocations motion, contributing to strengthen the alloy through the Orowan mechanism. Orowan hardening, σOR, was calculated using the equation proposed by Kocks and Ashby [43]:

$$\sigma_{ORedge} = \frac{1.69MGb^2}{4\pi} \cdot \frac{1}{\lambda} \cdot ln\frac{d}{2b} \text{ forc edge dislocations} \quad (4)$$

$$\sigma_{ORscrew} = \frac{\sigma_{ORedge}}{0.66} \text{ for screw dislocations} \quad (5)$$

where M is the Taylor's factor (6.5 for Mg [44]), G the shear modulus (17.3 GPa for Mg [45]), b the magnitude of the Burgers vector of slip dislocations (0.3196 nm [46]), d the average diameter of precipitates, and λ is the average spacing among precipitates on the relevant slip plane.

Thus, the total contribution to the yield stress increase associated with the Orowan process could be determined by:

$$\sigma_{OR} = \frac{\sigma_{ORscrew} + \sigma_{OREdge}}{2} \quad (6)$$

The calculated σOR value for the Mg-6Zn-1Y-1Ca alloy is 19 MPa. This proves almost negligible contribution due to the Orowan mechanism in this PM alloy.

4.3. Strengthening due to solid solution

According to EDS microanalyses, only zinc atoms are dissolved in the magnesium matrix (with an average concentration close to 2.4 at %). Since the hardening effect of 1 at% of Zn dissolved in the magnesium matrix has been estimated to increase about 2 MPa the yield stress of a binary Mg-Zn alloy [47], the solid solution hardening (σss) due to 2.4 at% has been calculated to be only 5 MPa.

4.4. Strengthening due to coarse second phases

Coarse second phases could provide an additional strengthening of the alloy. The yield stress σpar can be calculated by [Eq. (7)], which correlates yield stress and hardness of second-phase particles [48] as follows:

$$\sigma_{par} = \frac{H_v}{c} \quad (7)$$

being Hv the Vickers hardness of coarse second-phase particles and c the elastic constraint factor. For the present calculation, Hv has been considered as the Vickers hardness of the I-phase, taking the value of 192 MPa [35]. The elastic constraint factor c for a pyramidal indenter used for Vickers hardness measurements has a value of 0.3 [48]. Consequently, the yield stress of coarse I-phase (σpar) is estimated to be 640 MPa. Since the volume fraction of coarse I-phase is 15%, the contribution of this phase to the yield stress of the alloy is 97 MPa.

The yield stress of the alloy (σ0.2) was determined by substituting the calculated contributions for each individual strengthening mechanism in equation [Eq. (1)]. The obtained value is 454 MPa, only 7 MPa below that experimentally measured, within the experimental scatter. Fig. 11 illustrates contributions due to the different strengthening mechanisms for the Mg-6Zn-1Y-1Ca alloy. Major contribution arises from the fine grain size of the extruded alloy as result of the use of atomized powders, constituting more than 70% of the total yield stress. Contribution of the second phase particles is also important, about 21% of the yield stress. Minor contributions correspond to hardening induced by the precipitates inside the grains while the effect of dissolved atoms in the magnesium matrix is almost negligible. Furthermore, present analysis proves the irrelevant effect of texture on the yield stress of this PM alloy in spite its exhibits a non-negligible basal texture. This result is similar to that found in other magnesium alloys in which the strengthening induced mainly by grain size refinement precludes any contribution from texture component [22]. In Fig. 11 are also compared the strengthening due to these mechanisms in the same alloy processed through a conventional route of extrusion of as-cast ingots [22], hereafter designated as EI. The relevance of grain size refinement is considerably increased in the PM alloy because it constitutes more than 70% of the yield stress, while it only represents the 57% in the EI alloy. Although the volume fraction of second phases is almost twice in the PM alloy respect to the EI alloy, the stress due to second phase hardening is surprisingly only a little bit higher in the case of PM alloy (in absolute values, 97 MPa in PM alloy against 77 MPa in EI alloy) but its contribution, in percentage terms, is much higher in the EI alloy (37% and 21% for EI and PM alloys, respectively). The different volume fraction of second phases in the PM alloy is related to the different nature of second phases existing in PM and EI alloys. In the EI alloy, Ca and Y are tied in the Mg6Zn3Ca2 and W-phase, respectively, while they are distributed in the I-phase in the PM alloy. Minor amounts of Y and Ca are required to build the I-phase, one atom, compared to the two atoms required for the Mg6Zn3Ca2 and W-phase. Consequently, the same content of both elements render a higher volume fraction of second phases in PM alloy than in the EI alloy. In spite of the high volume fraction, effectiveness of strengthening due to I-phase is lower than that due to Mg6Zn3Ca2 and W-phase, because these phases are harder than I-phase [22]. Furthermore, load transfer from the matrix towards Mg6Zn3Ca2 and W-phase particles is favoured in the coarse/elongated shape presented by these phases compared with the fine equiaxed morphology of I-phase particles (most of them below 0.2–0.3 μm). This confirms that thermal treatment experienced by rapid atomized powders during the extrusion step promotes fine precipitation of a high volume fraction of I-phase particles. Such fine dispersion homogeneously distributed throughout the alloy acts as pinning points during the growth of

new recrystallized grains, rendering an extremely fine grain size, much smaller to that usually reported in magnesium alloys containing the I-phase [15,17,22,24,49–52]. As can be checked in Fig. 12, the yield stress of the alloy studied in this work is over the top, from our knowledge, of I-phase containing alloys in spite the concentration of alloying elements is almost identical or even lesser than those of some alloys included in the plot. This clearly indicates that strengthening of the alloys containing the I-phase derives predominantly from the grain size, being the hardening due to the I-phase considerably lower. Comparing values of alloys with compositions close to the Mg-Zn6-Y1-Ca1 alloy, this plot demonstrates that a decrease in the grain size from 8 to 0.8 μm enhances the yield stress about 200 MPa, but further refining up to 0.44 μm achieved in the present PM Mg-Zn6-Y1-Ca1 alloy induces an additional strengthening of 50 MPa.

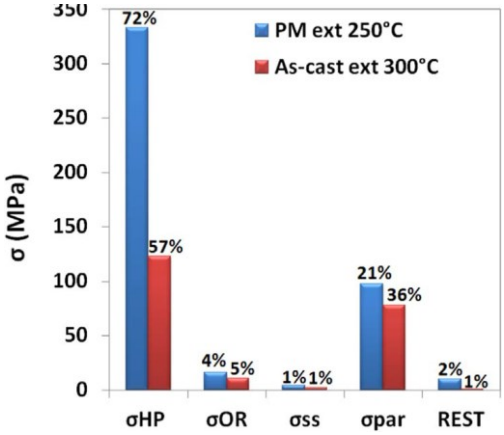

Fig. 11. Comparisons of the contributions to the yield stress (σ0.2) by the different hardening for the Mg-6Zn-1Y-1Ca processed by the powder metallurgy followed in this study with the same alloy processed through a conventional route involving extrusion of as-cast ingots [22].

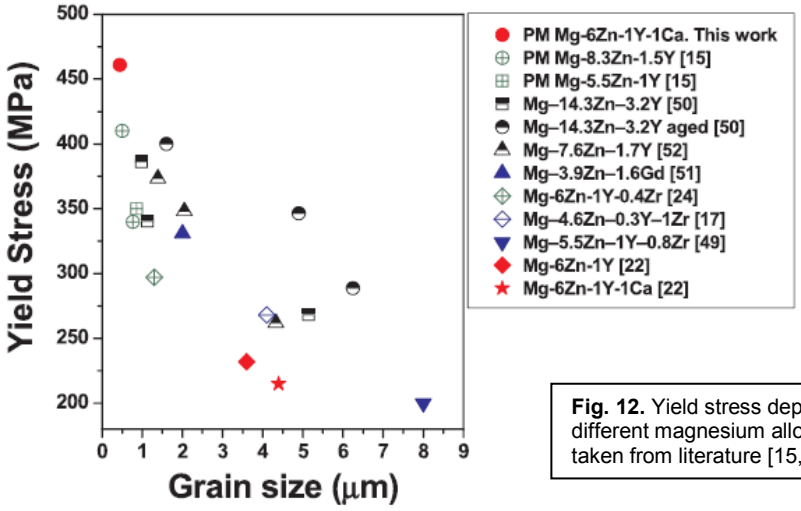

Fig. 12. Yield stress dependence with the grain size for different magnesium alloys reinforced by the I-phase taken from literature [15,17,22,24,47–50].

The analysis of stress exponent values in the 200–350 °C temperature range indicates that plastic deformation is controlled, depending on temperature and strain rate, by two different mechanisms. The first one is related to dislocations motion while the second one is grain boundary sliding (GBS). At 200 °C, GBS is favoured at low strain rates below 10−4 s−1, being the stress exponent almost 3. A similar behavior has been also reported for a fine-grained Mg–4.3 wt% Zn–0.7 wt% Y alloy, containing the I-phase, processed by equal channel angular pressing and tensile tested in the temperature range 250–350 °C [53]. A stress exponent of 3 is usually associated more with solute-drag/viscosous glide mechanism rather than GBS. In the present alloy, this could be indicative that deformation is not fully governed by GBS, at least at this temperature of 200 °C, existing a certain contribution of dislocation motion. This agrees with previous studies reporting that contribution of GBS to the total strain is comprised between 50% and 80% when GBS is the mechanism controlling the deformation [54,55]. Inversely, it has been reported that GBS can contribute significantly to the total strain when the deformation is governed by slip, enhancing the ductility of the alloy at expenses of a noticeable decrease in strength [56]. Probably, deviation of stress exponent values from 2 arises from the accommodation of the deformation, mainly at triple grain junctions, but also by the high volume

fraction of second phases at grain boundaries. Accommodation of such deformation cannot proceed easily as the strain rate is increased, so at strain rates higher than 3.10–4 s−1 the deformation becomes controlled by dislocation motion. The high value of the stress exponent indicates a significant interaction between dislocations and second-phase particles.

As the temperature increases, the interval for superplastic regime is shifted to higher strain rates. Moreover, the interval becomes broader, from 3.10−4 to 10−1 s−1, at 300 and 350 °C. The calculated activation energy corresponds to that of magnesium lattice self-diffusion. This result is unexpected because it differs from the values reported for other fine-grained magnesium alloys. According to the deformation maps for magnesium [58], the deformation mechanism is GBS controlled by grain boundary diffusion for alloys with fine grain sizes while GBS is controlled by lattice self-diffusion for those alloys with coarse grain sizes. Similar behaviour, even with activation energies below that of grain boundary diffusion, has been reported for fine-grained magnesium alloys [57–61]. Such different behaviour could be attributed to the presence of a high volume fraction of relatively coarse I-phase particles decorating grain boundaries of the magnesium matrix, which could disturb grain boundary transport phenomena there. In any case, matter transport in the alloy is very fast because of the fine grain size of the alloy, so lattice diffusion does not constitutes a factor limiting GBS mechanism even at temperatures as low as 200 °C, at which the GBS mechanism is controlled by grain boundary diffusion [57,60,61]. Superplastic flow implies grain rotation of magnesium grains whose movement is accommodated by I-phase particles located at grain boundaries, as it has been reported in the case of Mg-Ni-Y-RE alloys [11].

Tensile curves present a steady hardening along the entire superplastic regime, which can be associated with certain grain growth. Nevertheless, the high volume fraction of second phases attenuates grain growth during plastic deformation in such a way that grain size is always below the critical size for GBS can operate. Moreover, such hardening has a beneficial effect because it keeps uniform the plastic flow without the occurrence of necking which could lead to the premature failure of the material. As hardening increases with increasing the temperature, the maximum elongation to failure coincides with samples tested at 350 °C (477%).

5. Conclusions

From the present research the following conclusions can be drawn:

1. The use of atomized powders and 1% wt. Ca addition has a concomitant beneficial effect on the microstructure of the extruded alloy. Fine precipitation of I-phase during the extrusion prevents grain coarsening of the magnesium matrix.
2. The volume fraction of second phases is almost to times higher than that found in the same alloy processed by extrusion of as-cast rods.
3. Heating at temperatures beyond the temperature for Mg6Zn3Ca2 formation could lead to a decrease in the volume fraction of second phases pinning grain boundaries, inducing accelerated grain growth.
4. High yield stress of 461 MPa at room temperature comes from the fine grain size of the magnesium matrix, constituting more than 70% of the total contribution. Hardening due to second phase particles supposes only the 21% of the yield stress. Strengthening due to Orowan mechanism and dissolved atoms in the magnesium matrix are almost negligible.
5. The alloy exhibits superplastic behaviour by grain boundary sliding between 200 and 350 °C in a wide interval of strain rates, with a maximum elongation of 477% at 350 °C. Deformation is controlled by lattice self-diffusion instead of grain boundary diffusion reported during superplastic deformation of fine-grained magnesium alloys.

Acknowledgments

We would like to acknowledge the financial support of the Spanish Ministry of Economy and Competitiveness under project MAT2012-34135 and Fondo Europeo de Desarrollo Regional, FEDER MAT2012-34135. We would like to acknowledge the expert support of A. García and A. Tomás for assistance with TEM and SEM. and the support of M. Acedo for assistance with the extrusion processing. The Deutches Elektronen-Synchrotron DESY is acknowledged for the provision of beamtime at the P07 beamline of the Petra III synchrotron facility in the framework of proposal I-20140198 EC.

References

[1] A. Luo, M.O. Pekguleryuz, Cast magnesium alloys for elevated temperature applications, J. Mater. Sci. 29 (1994) 5259–5271, http://dx.doi.org/10.1007/BF01171534.
[2] I.J. Polmear, LightAlloys, 3rd ed., Arnold, London, 1995.
[3] M.M. Avedesian, H. Baker, Magnesium and Magnesium Alloys, ASM International, Materials Park, Ohio, 1999.
[4] D. Letzig, J. Swiostek, J. Bohlen, P.A. Beaven, K.U. Kainer, Wrought magnesium alloys for structural applications, Mater. Sci. Technol. 24 (2008) 991–996, http://dx.doi.org/10.1179/174328407X213080.
[5] A.A. Luo, Recent magnesium alloy development for elevated temperature applications, Int. Mater. Rev. 49 (2004) 13–30, http://dx.doi.org/10.1179/095066004225010497.
[6] S. González, G. Garcés, P. Adeva, P. Pérez, Influence of processing route on microstructure and mechanical properties of Mg-Ni-Y-RE alloys, Mater. Charact. 64 (2012) 53–61, http://dx.doi.org/10.1016/j.matchar.2011.12.001.
[7] K. Liu, X. Wang, K. Wen, Effect of isothermal homogenization on microstructure and mechanical properties of the Mg–5Y–4Gd–0.5Zn–0.4Zr alloy, Mater. Des. 52 (2013) 1035–1042, http://dx.doi.org/10.1016/j.matdes.2013.06.048.
[8] W. Mo, L. Zhang, G. Wu, Y. Zhang, W. Liu, C. Wang, Effects of processing parameters on microstructure and mechanical properties of squeeze-cast Mg–12Zn–4Al–0.5Ca alloy, Mater. Des. 63 (2014) 729–737, http://dx.doi.org/10.1016/j.matdes.2014.07.005.
[9] G. Garcés, M.A. Muñoz-Morris, D.G. Morris, P. Pérez, P. Adeva, Optimization of strength by microstructural refinement of MgY2Zn1 alloy during extrusion and ECAP processing, Mater. Sci. Eng. A614 (2014) 96–105, http://dx.doi.org/10.1016/j.msea.2014.07.012.
[10] T. XingHe, W.C. Keat How, J.C. Kwok Weng, R.K. Wai Onn, M. Gupta, Development of high-performance quaternary LPSO Mg–Y–Zn–Al alloys by disintegrated melt deposition technique, Mater. Des. 83 (2015) 443–450, http://dx.doi.org/10.1016/j.matdes.2015.06.041.
[11] S. González, P. Pérez, G. Garcés, P. Adeva, Influence of the processing route on the mechanical properties at high temperatures of Mg-Ni-Y-RE alloys containing LPSOphases, Mater. Sci. Eng. A673 (2016) 266–279, http://dx.doi.org/10.1016/j.msea.2016.07.077.
[12] A. Singh, M. Watanabe, A. Kato, A.P. Tsai, Microstructure and strength of quasicrystal containing extruded Mg–Zn–Y alloys for elevated temperature application, Mater. Sci. Eng. A 385 (2004) 382–396, http://dx.doi.org/10.1016/j.msea.2004.06.059.
[13] J.Y. Lee, H.K. Lim, D.H. Kim, W.T. Kim, D.H. Kim, Effect of volume fraction of quasicrystal on the mechanical properties of quasicrystal-reinforced Mg–Zn–Y alloys, Mater. Sci. Eng. A 449–451 (2007) 987–990, http://dx.doi.org/10.1016/j.msea.2006.03.141.
[14] G. Garcés, A. Müller, E. Oñorbe, P. Pérez, P. Adeva, Effect of hot forging on the microstructure and mechanical properties of Mg–Zn–Y, J. Mater. Proc. Technol. 206 (2008) 99–105, http://dx.doi.org/10.1016/j.jmatprotec.2007.12.014.
[15] E. Mora, G. Garcés, E. Oñorbe, P. Pérez, P. Adeva, High-strength Mg-Zn-Y alloys produced by powder metallurgy, Scr. Mater. 60 (2009) 776–779, http://dx.doi.org/10.1016/j.scriptamat.2009.01.012.
[16] N. Tahreen, D.F. Zhang, F.S. Pan, X.Q. Jiang, D.Y. Li, D.L. Chen, Hot deformation and processing map of an as-extruded Mg-Zn-Mn-Y alloy containing I and W phases, Mater. Des. 87 (2015) 245–255, http://dx.doi.org/10.1016/j.matdes.2015.08.023.
[17] X. Chen, L. Liu, J. Liu, F. Pan, Microstructure, electromagnetic shielding effectiveness and mechanical properties of Mg–Zn–Y–Zr alloys, Mater. Des. 65 (2015) 360–369, http://dx.doi.org/10.1016/j.matdes.2014.09.034.
[18] K. Hagihara, A. Kinoshita, Y. Sugino, M. Yamasaki, Y. Kawamura, H.Y. Yasuda, Y. Umakoshi, Effect of long-period stacking ordered phase on mechanical properties of Mg97Zn1Y2 extruded alloy, Acta Mater. 58 (2010) 6282–6293, http://dx.doi.org/10.1016/j.actamat.2010.07.050.
[19] M. Okayasu, S. Takeuchi, M. Matsushita, N. Tada, M. Yamasaki, Y. Kawamura, Mechanical properties and failure characteristics of cast and extruded Mg97Y2Zn1 alloys with LPSO phase, Mater. Sci. Eng. A652 (2016) 14–29, http://dx.doi.org/10.1016/j.msea.2015.11.069.
[20] P. Pérez, J. Medina, G. Garcés, P. Adeva, Influence of Y-CeMM ratio on the microstructure and mechanical properties of Mg95Zn2(Y,CeMM)3 alloys, Intermetallics 31 (2012) 196–201, http://dx.doi.org/10.1016/j.intermet.2012.07.005.
[21] G. Garcés, D.G. Morris, M.A. Muñoz-Morris, P. Perez, D. Tolnai, C. Mendis, A. Stark, H.K. Lim, S. Kim, N. Shell, P. Adeva, Plasticity analysis by synchrotron radiation in a Mg97Y2Zn1 alloy with bimodal grain structure and containing LPSO phase, Acta Mater. 94 (2015) 78–86, http://dx.doi.org/10.1016/j.actamat.2015.04.048.
[22] J. Medina, P. Pérez, G. Garcés, P. Adeva, Effects of calcium, manganese and cerium rich mischmetal additions on the mechanical properties of extruded Mg-Zn-Y alloy reinforced by quasicrystalline I-phase, Mater. Charact. 129 (2017) 195–206, http://dx.doi.org/10.1016/j.matchar.2017.04.033.
[23] T. Ebert, K.U. Kainer, Rapid solidification and special processes for processing magnesium alloys, in: K.U. Kainer (Ed.), Magnesium – Alloys and Technology, 2003, pp. 164–183, ⟨http://dx.doi.org/10.1002/3527602046.ch10⟩.
[24] A. Müller, G. Garcés, P. Pérez, P. Adeva, Grain refinement of Mg–Zn–Y alloy reinforced by an icosahedral quasicrystalline phase by severe hot rolling, J. Alloy. Compd. 443 (2007) L1–L5, http://dx.doi.org/10.1016/j.jallcom.2006.10.006.
[25] M. Yang, J. Zhang, T. Guo, Effects of Ca addition on as-cast microstructure and mechanical properties of Mg–3Ce–1.2Mn–1Zn (wt%) magnesium alloy, Mater. Des. 52 (2013) 274–283, http://dx.doi.org/10.1016/j.matdes.2013.05.049.
[26] F. Li, W.Y. Peh, V. Nagarajan, M.K. Ho, A. Danno, B.W. Chua, M.J. Tan, Development of non-flammable high strength AZ91 + Ca alloys via liquid forging and extrusion, Mater. Des. 99 (2016) 37–43, http://dx.doi.org/10.1016/j.matdes.2016.03.014.
[27] S. Tekumalla, M. Gupta, An insight into ignition factors and mechanisms of magnesium based materials: a review, Mater. Des. 113 (2017) 84–98, http://dx.doi.org/10.1016/j.matdes.2016.09.103.

[28] C. Sanchez, G. Nussbaum, P. Azavant, H. Octor, Elevated temperature behaviour of rapidly solidified magnesium alloys containing rare earths, Mater. Sci. Eng. A221 (1996) 48–57, http://dx.doi.org/10.1016/S0921-5093(96)10469-X.
[29] G. Garcés, F. Domínguez, P. Pérez, G. Caruana, P. Adeva, Effect of extrusion temperature on the microstructure and plastic deformation of PM-AZ92, J. Alloy. Compd. 422 (2006) 293–298, http://dx.doi.org/10.1016/j.jallcom.2005.11.069.
[30] P. Pérez, G. Garcés, P. Adeva, Influence of texture on the mechanical properties of commercially pure magnesium prepared by powder metallurgy, J. Mater. Sci. 42 (2007) 3969–3976, http://dx.doi.org/10.1007/s10853-006-1301-3.
[31] A. Elsayed, K. Kondoh, H. Imai, J. Umeda, Microstructure and mechanical properties of hot extruded Mg–Al–Mn–Ca alloy produced by rapid solidification powder metallurgy, Mater. Des. 31 (2010) 2444–2453, http://dx.doi.org/10.1016/j.matdes.2009.11.054.
[32] S. Cabeza, G. Garcés, P. Pérez, P. Adeva, Microstructure and mechanical behavior of powder metallurgy Mg98.5Gd1Zn0.5 alloy, Metall. Mater. Trans. A45 (2014) 3222–3231, http://dx.doi.org/10.1007/s11661-013-2041-z.[33] D.K. Xu, E.H. Han, Effects of icosahedral phase formation on the microstructure and mechanical improvement of Mg alloys: a review, Prog. Mater. Sci. Mater. 22 (2012)364–385, http://dx.doi.org/10.1016/j.pnsc.2012.09.005.
[34] A. Inoue, Y. Kawamura, M. Matsushita, K. Hayashi, J. Koike, Novel hexagonal structure and ultrahigh strength of magnesium solid solution in the Mg–Zn–Y system, J. Mater. Res. 16 (2001) 1894–1900.
[35] Y.Z. Du, M.Y. Zheng, X.G. Qiao, K. Wu, X.D. Liu, G.J. Wang, X.Y. Lv, Microstructure and mechanical properties of Mg–Zn–Ca–Ce alloy processed by semi-continuous casting, Mater. Sci. Eng. A582 (2013) 134–139, http://dx.doi.org/10.1016/j.msea.2013.06.027.
[36] M. Hradilová, D. Vojtěch, J. Kubásek, J. Čapek, M. Vlach, Structural and mechanical characteristics of Mg–4Zn and Mg–4Zn–0.4Ca alloys after different thermal and mechanical processing routes, Mater. Sci. Eng. A586 (2013) 284–291, http://dx.doi.org/10.1016/j.msea.2013.08.008.
[37] J. Medina, P. Pérez, G. Garcés, D. Tolnai, A. Stark, N. Schell, P. Adeva, Microstructural changes in an extruded Mg-Zn-Y alloy reinforced by quasicrystalline I-phase by small additions of calcium, manganese and cerium-rich mischmetal, Mater. Charact. 118 (2016) 186–198, http://dx.doi.org/10.1016/j.matchar.2016.05.019.
[38] Y. Zhang, X. Zeng, L. Liu, C. Lu, H. Zhou, Q. Li, Y. Zhu, Effects of yttrium on microstructure and mechanical properties of hot-extruded Mg-Zn-Y-Zr alloys, Mater. Sci. Eng. A373 (2004) 320–327, http://dx.doi.org/10.1016/j.msea.2004.02.007.
[39] X. Zeng, Y. Zhang, C. Lu, W. Ding, Y. Wang, Y. Zhu, Precipitation behavior and mechanical properties of a Mg–Zn–Y–Zr alloy processed by thermo-mechanical treatment, J. Alloy. Compd. 395 (2005) 213–219, http://dx.doi.org/10.1016/j.jallcom.2004.10.070.
[40] B. Zhang, Y. Wang, L. Geng, C. Lu, Effects of calcium on texture and mechanical properties of hot-extruded Mg–Zn–Ca alloys, Mater. Sci. Eng. A539 (2012) 56–60, http://dx.doi.org/10.1016/j.msea.2012.01.030.
[41] E.A. Brandes, G.B. Brook, Smithells Metals Reference Book, (1992).
[42] P. Andersson, C.H. Cáceres, J. Koike, Hall-Petch parameters for tension and compression in cast Mg, Mater. Sci. Forum 419 (2003) 123–128, http://dx.doi.org/10.4028/www.scientific.net/MSF.419-422.123.
[43] M.A. Morris, D.G. Morris, An analysis of the thermal and mechanical stability of rapidly solidified Cu-Mn-B alloys, Acta Metall. 36 (1988) 1187–1199, http://dx.doi.org/10.1016/0001-6160(88)90171-X.
[44] B. Bhattacharya, M. Niewczas, Work-hardening behaviour of Mg single crystals oriented for basal slip, Philos. Mag. 91 (2011) 2227–2247, http://dx.doi.org/10.1080/14786435.2011.555783.
[45] J.G. Kaufman, A.S.M. Ready, Reference: Properties and Units for Engineering Alloys, ASM International, United States of America, 1997, p. 168.
[46] C.H. Cáceres, P. Lukáč, Strain hardening behaviour and the Taylor factor of pure magnesium, Philos. Mag. 88 (2008) 977–989, http://dx.doi.org/10.1080/14786435.2011.555783.
[47] I. Toda-Caraballo, E.I. Galindo-Nava, P.E.J. Rivera-Díaz-delCastillo, Understanding the factors influencing yield strength on Mg alloys, Acta Mater. 75 (2014) 287–296, http://dx.doi.org/10.1016/j.actamat.2014.04.064.
[48] C.H. Cáceres, J.R. Griffiths, A.R. Pakdel, C.J. Davidson, Microhardness mapping and the hardness-yield strength relationship in high-pressure diecast magnesium alloy AZ91, Mater. Sci. Eng. A402 (2005) 258–268, http://dx.doi.org/10.1016/j.msea.2005.04.042.
[49] D.K. Xu, L. Liu, Y.B. Xu, E.H. Han, Effect of microstructure and texture on the mechanical properties of the as-extruded Mg–Zn–Y–Zr alloys, Mater. Sci. Eng. A443 (2007) 248–256, http://dx.doi.org/10.1016/j.msea.2006.08.037.
[50] A. Singh, Y. Osawa, H. Somekawa, T. Mukai, Ultra-fine grain size and isotropic very high strength by direct extrusion of chill-cast Mg–Zn–Y alloys containing quasicrystal phase, Scr. Mater. 64 (2011) 661–664, http://dx.doi.org/10.1016/j.scriptamat.2010.12.016.
[51] H. Huang, C. Chen, Z. Wang, Y. Li, G. Yuan, Effect of pretreatment and annealing on microstructure and mechanical properties of Mg–1.5Zn–0.25Gd (at%) alloys reinforced with quasicrystal, Mater. Sci. Eng. A581 (2013) 73–82, http://dx.doi.org/10.1016/j.msea.2013.06.003.
[52] A. Singh, Y. Osawa, H. Somekawa, T. Mukai, Effect of microstructure on strength and ductility of high strength quasicrystal phase dispersed Mg–Zn–Y alloys, Mater. Sci. Eng. A611 (2014) 242–251, http://dx.doi.org/10.1016/j.msea.2014.05.091.
[53] M.Y. Zheng, S.W. Xu, K. Wu, S. Kamado, Y. Kojima, Superplasticity of Mg-Zn-Y alloy containing quasicrystal phase processed by equal channel angular pressing, Mater. Lett. 61 (2007) 4406–4408, http://dx.doi.org/10.1016/j.matlet.2007.02.013.
[54] R.Z. Valiev, O.A. Kaybishev, On the quantitative evaluation of superplastic flow mechanism, Acta Metall. 31 (1983) 2121–2128, http://dx.doi.org/10.1016/0001-6160(83)90031-7.
[55] B.P. Kashyap, A. Arieli, A.K. Mukherjee, Microstructural aspects of superplasticity, J. Mater. Sci. 20 (1985) 2661–2686, http://dx.doi.org/10.1007/BF00553028.

[56] M. Mabuchi, Y. Chino, H. Iwasaki, Low temperature superplasticity of magnesium alloys, Mater. Trans. 43 (2002) 2063–2068.
[57] W.J. Kim, S.W. Chung, C.S. Chung, D. Kum, Superplasticity in thin magnesium alloy sheets and deformation mechanism maps for magnesium alloys at elevated temperatures, Acta Mater. 49 (2001) 3337–3345, http://dx.doi.org/10.1016/S1359-6454(01)00008-8.
[58] H. Watanabe, T. Mukai, M. Mabuchi, K. Higashi, Superplastic deformation mechanism in powder metallurgy magnesium alloys and composites, Acta Mater. 49 (2001) 2027–2037, http://dx.doi.org/10.1016/S1359-6454(01)00101-X.
[59] H. Watanabe, T. Mukai, K. Ishikawa, K. Higashi, Low temperature superplasticity of a fine-grained ZK60 magnesium alloy processed by equal-channel-angular extrusion, Scr. Mater. 46 (2002) 851–856, http://dx.doi.org/10.1016/S1359-6462(02)00064-7.
[60] V.N. Chuvil'deev, T.G. Nieh, M.Yu Gryaznov, A.N. Sysoev, V.I. Kopylov, Low-temperature superplasticity and internal friction in microcrystalline Mg alloys processed by ECAP, Scr. Mater. 50 (2004) 861–865, http://dx.doi.org/10.1016/j.scriptamat.2003.12.003.
[61] V.N. Chuvil'deev, T.G. Nieh, M.Yu Gryaznov, V.I. Kopylov, A.N. Sysoev, Superplasticity and internal friction in microcrystalline AZ91 and ZK60 magnesium alloys processed by equal-channel angular pressing, J. Alloy. Compd. 378 (2004) 253–257, http://dx.doi.org/10.1016/j.jallcom.2003.10.062.